SMC Project

NOTE

CEA-IRFU-SIS
CERN-AT-MCS
RAL-STFC
LBNL

Date: June 4 2008
v 1.0

CEA N/Ref: IRFU/SIS/1467/08/PM
EDMS Id: 926137

NED Short Model Coils project:
Technical Note on Magnetic Design

Pierre Manil[1], Federico Regis[3], James Rochford[4],
Elwyn Baynham[4], Simon Canfer[4], Shlomo Caspi[5], Arnaud Devred[6], George Ellwood[4], Hélène Félice[5], Paolo Ferracin[5], Paolo Fessia[3], Peter Ford[4], François-Paul Juster[2], François Nunio[1], Gijsbert de Rijk[3], Pierre Védrine[2]

[1] *CEA/DSM/IRFU/SIS, Gif-sur-Yvette, France*
[2] *CEA/DSM/IRFU/SACM, Gif-sur-Yvette, France*
[3] *CERN/AT, CH-1211 Genève 23, Switzerland*
[4] *RAL/STFC, Harwell Science and Innovation Campus, Didcot, United Kingdom*
[5] *LBNL, UC Berkeley, California, United States*
[6] *ITER IO, Cadarache, St. Paul-lez-Durance, France*

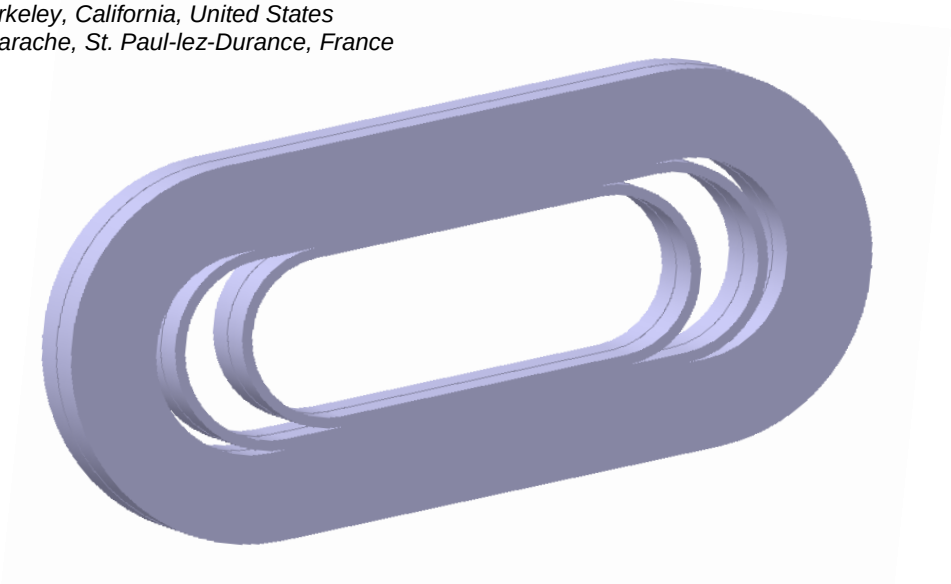

Abstract

The **Short Model Coils** working group was set in February 2007 within the context of the Next European Dipole (NED) Joint Research Activity. The aim of the collaborative program is to design, manufacture and test Nb_3Sn racetrack subscale coils in dipole configuration. An adapted support structure will be used to perform training studies while investigating pre-stress influence on coil behaviour and quench triggering. It needs to have the ability to apply very high as well as very low pre-stresses on the coil pack, in the three directions. Such a system should help define the mechanical stress limit on different coil pack configurations with innovative insulations. SMC studies will utilise the experience of Berkeley's SD01 subscale coil, which is pre-stressed by a shell-based structure and is using bladders and keys.

This paper details the initial magnetic optimization of the test structure. It describes the magnetic field specifications and their consequences on the coil parameterization and design. After cross-checking 3D nonlinear models using up to four different finite elements codes (CAST3M, ANSYS, OPERA, ROXIE), the reasons behind the chosen coil parameters are given. The optimization exercise has led to a redesign of the coil, to use iron surrounding parts and to make use of four end spacers to get a peak field higher than 13 T located on conductor, in the centre of the straight section, with high uniformity.

Contents

1- Overview of the Short Model Coils project

1.1- Goal of the project

Particle accelerators are key tools for particle physics, as they allow researchers to explore smaller and smaller components of matter by colliding elementary particles at very high energies. The beam energy is proportional to the curvature radius, which depends on the magnetic field created by dipole magnets. To reach the very high magnetic fields required to produce the high energies of collision, superconducting materials are used. Their lack of electrical resistance at low temperatures makes the use of very high current densities possible. As an example, the Large Hadron Collider (LHC) at CERN will reach collision energies of a magnitude of 14 TeV thanks to NbTi dipoles producing a field higher than 8 T in a 56 mm aperture.

Future LHC upgrades requiring higher fields in larger apertures will demand the use of a superconductor with greater performance compared to NbTi. The use of Nb_3Sn is one possibility, allowing peak fields in the conductor up to 24 T to be sustained. However, this material remains very sensitive to mechanical constraints. Its upper working stress limit, which is estimated around 150 MPa, is not precisely known. Furthermore, the behaviour of Nb_3Sn cables in wound coils is not fully understood.

The goal of the Short Model Coils (SMC) working group, within the CARE NED[1] context, is to create a short-model Nb_3Sn coil testing device [1].

The function of this device is the application of variable pre-stress levels to the coil in order to study the degradation of the magnetic properties of the superconducting cable due to different levels of stresses. The use of bladders and keys has been retained from Berkeley's SD01 coil, to provide an adequate on-plane pre-stress [2,3,4]. The longitudinal pre-stress will be applied by means of rods. Another requirement is the device needs to be easy to assemble and disassemble, to allow the testing of different types of cable in the subscale racetrack test dipoles. Additionally the SMC wishes to test different conductor insulation methods *i.e.* so-called "conventional insulation" (glass fibre + organic matrix), and more innovative ceramic insulation [5].

The SMC group will supervise the design and manufacture of the coils to be tested, of their support and testing structure and of the associated tooling. The SMC group comprises four laboratories: CERN/AT-MCS (CH), RAL (UK), CEA/IRFU/SIS with support from CEA/IRFU/SACM (FR) and LBNL (US). The magnetic optimization phase has been shared by all; however the role of each laboratory has been chosen to build on their natural strengths and areas of interest.

[1] NED is an acronym for Next European Dipole. This Joint Research Activity (JRA) was launched on January 2004 to promote the development of high performance Nb_3Sn conductors in collaboration with European industry and to assess the suitability of Nb_3Sn technology to the next generation of accelerator magnets. The target is to reach a non-copper critical current density of 1500 $A.mm^{-2}$ at 4.2 K and 15 T, an aperture of 88 mm and a conductor peak around 15 T.

1.2- A precedent study: SD01 coil

A similar assembly to the SMC short sub coil test assembly has already been realized at Lawrence Berkeley National Laboratory (LBNL), in the US. This work has been followed at CEA Saclay by Hélène Félice (PhD work, 2003-2006), who is a collaborator within the SMC working group and a LARP[2] correspondent [6].

The SD01 goal was to study the pre-stress influence on Nb_3Sn dipole magnets, and how this affected their training. Pre-stress was applied in the lateral and longitudinal directions.

As showed on picture 1.2.1, SD01 contains five main elements: the **superconducting coil pack** (in the centre), **two pre-stress pads** – which also play a magnetic role (as shown later), the **surrounding yoke** and **an external aluminium shell**. The cryogenic system is not illustrated since it is classical.

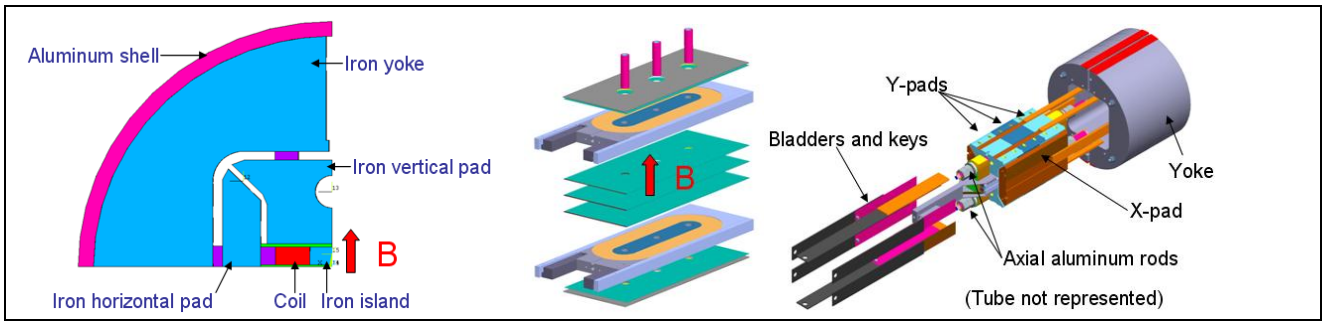

***Fig. 1.2.1**: SD01 structure principle*

Part of the pre-stress is applied during cool-down, by utilising the thermal contraction of the aluminium shell[3] and of the axial rods. The remainder of the initial load is applied by stainless steel bladders, which are replaced by steel keys when the target pre-stress level is achieved (this makes them different from LHC bladders which are never removed). This loading principle will be kept for SMC.

Studies carried out by Hélène Félice have validated the general principle of the assembly, and have proved its mechanical effectiveness for training studies. She has highlighted the need for increasing the pre-stress range and improving the coil instrumentation to achieve more accurate results. Some pre-stress losses have been observed on SD01. These need to be taken into account to avoid an assembly overloading to get the normal pre-stress level, as it could damage the coil. A thorough design, taking into account the fabrication tolerances is required. Last but not least, within SD01 the magnetic peak field is obtained on the racetrack coil ends. The desire here is to test the maximum admissible stress on the undeformed cable, *i.e.* mechanically homogeneous, **to do this the peak magnetic field is required in the straight section: this requires a magnetic re-design**. To achieve this, the SMC will adapt the iron parts, and to explore the use of end spacers.

To summarise, the SMC working group will use the SD01 test concept as a starting point and will perform an optimisation to improve on it magnetically and mechanically.

[2] US LHC Accelerator Research Program
[3] high thermal coefficient around 4.5 $mm.m^{-1}$ between 293 and 4.2 K

1.3- Magnetic specifications

The main design criteria of the SMC are:

1. Suitability of the magnetic field
2. Mechanical sustainability; variability of the pre-stress
3. Easiness of mounting and testing
4. Using the support with different coil packs
5. Adapted instrumentation

This paper concentrates on point 1.

The main magnetic conception constraint is to get the peak field B_{max} in the centre of the straight section of the racetrack with the aim of obtaining the critical conditions for the superconductor in this region, where the conductor is close to being as mechanically homogeneous as possible. The magnetic field on coil ends should be 0.5 T lower than the field on the straight section, where it should approach 13 T at short sample limit.

Moreover the uniformity of the field in this zone should be 1% the peak value, and this region should exist from the centre of the dipole over a full twist pitch length (approximately 60 mm) of the conductor.

In addition to these fundamental magnetic specifications there are further constraints. The working current is limited to 20 kA by the available power supply. The overall dimensions for the coil are driven by the reaction furnace available, and the test cryostat available, as discussed later. Additionally there are implicit cost constraints.

Those specifications are summed up in the table 1.3.1:

Parameter	Name	Unit	Value	Notes
Magnetic field constraints				
Peak field	B_{max}	T	in straight section	
B_{ss} - B_{end}	ΔB_{ss}	T	≥ 0.5	
Peak straight section field	B_{ss}	T	~ 13	
Uniform field zone length	$L_u^{1\%}$	mm	~ 60	*at 1%*
$B_{end}^{(inner\ pack)}$ - $B_{end}^{(outer\ pack)}$	ΔB_{end}	T	≥ 0.5	
End field	B_{end}	T	none	
Central field	B_0	T	none	
Facilities Constraints				
Current	I_{ss}	kA	≤ 20	
Overall length	L_{tot}	mm	≤ **	*with tooling*
Overall width	w_{tot}	mm	≤ **	*with tooling*
Furnace temperature uniformity	ΔT	°C	±2.5	*on L_{tot}*

*** Dimension constraints depend on the furnace used*

***Tab. 1.3.1**: NED SMC magnetic specifications*

1.4- Assembly architecture

For SD01 the test architecture has proven to be efficient [6]. It is for the large part retained here. The test device will still consist of five main parts: **coil pack, horizontal (X) pad, vertical (Y) pad, yoke and tube**. The use of keys and bladders is also retained (§ 1.2). However the parts' shapes, dimensions and materials (iron - no iron) will be discussed and adapted. A baseline representation of the system is proposed on picture 1.4.1.

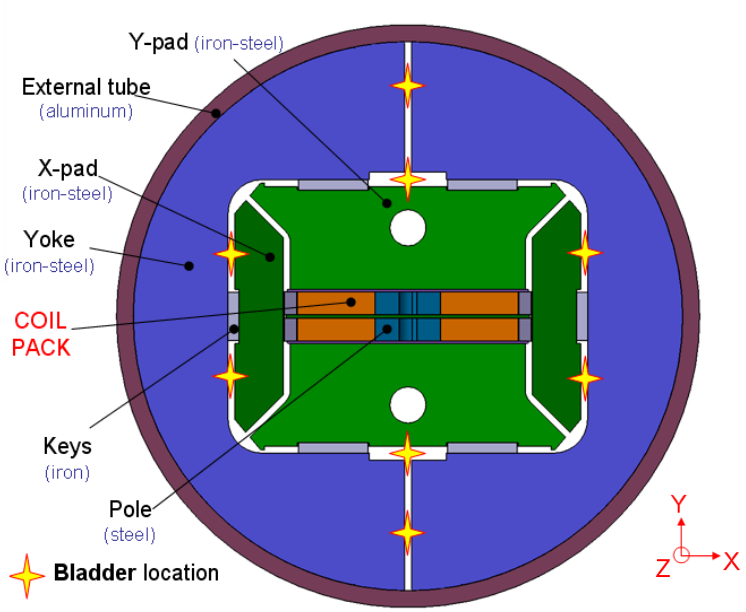

***Fig. 1.4.1**: NED SMC mechanical baseline structure (2D cut)*

In order to respect § 1.3 specifications, the coil will undergo most of the changes. Nevertheless, the choice of a racetrack configuration with two planar double-pancakes as described in § 2.2 is maintained.

1.5- Steps

NED SMC study was launched in February 2007. The desire is to achieve the coil optimization, conceptual design, mechanical design, cable fabrication, coils reaction / impregnation, integration of the complete test system, culminating in the first tests (a *dummy coil* first and then a superconducting coil) all within eighteen months.

After the definition of the basic system, the first step was to fix the coil geometry corresponding to the needs of the SMC project. This phase has taken five months and many modelling iterations, shared between different laboratories and codes to achieve; it is summarized in this Technical Note.

The following phases will consist of tooling design, mechanical conception and detailed design.

2- Magnetic optimization steps

Although the system will be used to test different coil geometries, the first step in the optimization was to define a baseline coil. It assumed conventional glass fibre + epoxy insulation.

2.1- Cable choice

For the basic racetrack configuration, the cable is assumed to be 14-strands Nb_3Sn Rutherford-type cable with a strand diameter of 1.25 mm. The rectangular cable section is 9.7 x 2.2 mm plus 0.2 mm per face for insulation (figure 2.1.3). Target practical strand current density at 12 T is 2500 $A.mm^{-2}$ that corresponds to a current of 17180 A in cable section, *i.e.* an engineering density J_{eng} around 654 $A.mm^{-2}$. Critical current slope is experimentally known around 12 T. Those properties are summed up in table 2.1.1:

Parameter	Name	Unit	Value	d.o.f.	Notes
Cable					
Number of strands	$\mathbf{N_{str}}$	/	14	fixed	
Strand diameter	$\mathbf{Ø_{str}}$	mm	1.25	fixed	
Cu / nCu rate	$\mathbf{r_{Cu/nCu}}$	/	1.25	fixed	
Twist pitch	**p**	mm	60	fixed	*approx.*
Cable width	$\mathbf{w_{cbl}}$	mm	9.7	fixed	
Thickness at 20 MPa	$\mathbf{e_{cbl}}$	mm	2.20	fixed	
Insulation thickness	$\mathbf{e_{ins}}$	mm	0.2	fixed	*per face*
Critical current slope	$\boldsymbol{\alpha_c}$	$A.T^{-1}$	3 435	fixed	*at 12T*
I_c target (3000 $A.mm^{-2}$)	I_c^{trg}	A	(20 608)	calculated	*at 12T; 4.2K (1)*
I_c practical (2500 $A.mm^{-2}$)	I_c^{12}	A	17 180	calculated	*at 12T; 4.2K (1)*
Cable J_{eng} at 2500 $A.mm^{-2}$	J_{eng}	$A.mm^{-2}$	654.227	calculated	*(2)*

(1) $$I_c^{trg} = 3000 \times \pi . \left(\frac{Ø_{str}}{2}\right)^2 \times \frac{N_{str}}{1 + r_{Cu/nCu}} \times (1 - 0.1) \qquad I_c^{12} = 2500 \times \pi . \left(\frac{Ø_{str}}{2}\right)^2 \times \frac{N_{str}}{1 + r_{Cu/nCu}} \times (1 - 0.1)$$

(2) $$J_{eng} = \frac{I_c^{12}}{(w_{cbl} + 2.e_{ins}).(e_{cbl} + 2.e_{ins})}$$

***Tab. 2.1.1**: NED SMC cable properties*

The cable differs from the SD01 case, as shown in table 2.1.2:

NED Cable	Name	Unit	NED SMC	SD01
Number of strands	$\mathbf{N_{str}}$	/	14	20
Strand diameter	$\mathbf{Ø_{str}}$	mm	1.25	0.7
Cu / nCu rate	$\mathbf{r_{Cu/nCu}}$	/	1.25	0.8
Twist pitch	**p**	mm	60	?
Cable width	$\mathbf{w_{cbl}}$	mm	9.7	7.793
Thickness at 20 MPa	$\mathbf{e_{cbl}}$	mm	2.20	1.275
Insulation thickness (per face)	$\mathbf{e_{ins}}$	mm	0.2	0.1
Critical strand current density	J_{str}	$A.mm^{-2}$	2500	2200
Cable practical J_{eng} at J_{str}	J_{eng}	$A.mm^{-2}$	654.227	718.138

***Tab. 2.1.2**: comparison between SMC and SD01 cable properties*

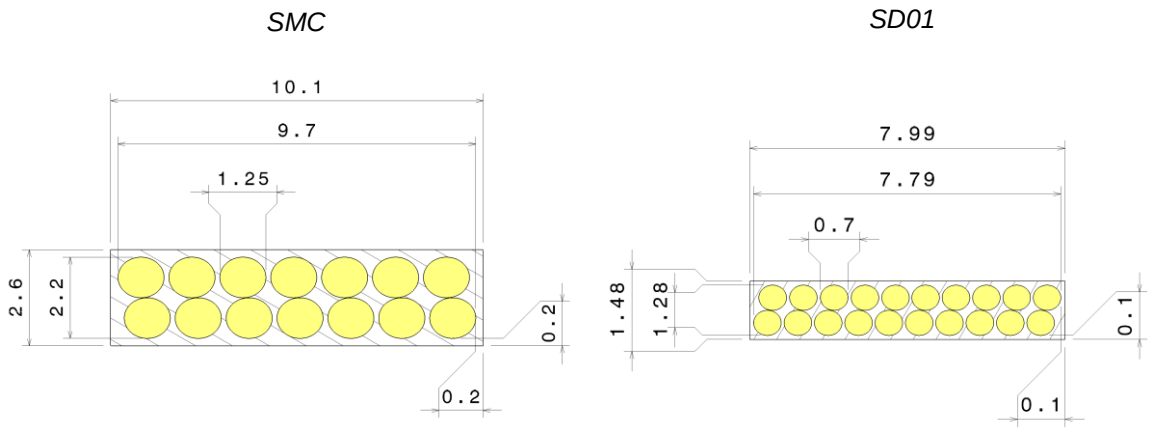

***Fig. 2.1.3**: comparison between SMC and SD01 cable cross-section (in mm)*

2.2- Optimization starting point

The subscale coils are racetrack-shaped. They are made of two Nb_3Sn cable layers wound around a metallic island (*double pancake* configuration). A thin insulation is placed between both pancakes. The whole dipole magnet consists in **two double pancakes** separated by a thicker midplane insulation layer made of G10.

First task is to parameterize the basic coil pack geometry. Nine relevant parameters are identified at first (see table 2.2.1): turns numbers for each pack, island half-width (*i.e.* minimal bending radius), outer radius (which results from other parameters), straight section length, spacer length and insulation thicknesses. Later the need for a second end spacer is justified, leading to two more parameters: mid-pack turns number and spacer's length.

Parameter	Name	Unit	Value	d.o.f.	Notes
Coil Pack – Double Pancake Configuration					
Turns number	$\mathbf{N_{tot}}$	/	to be determined	variable	
Inner turns number	$\mathbf{N_{int}}$	/	to be determined	variable	
Outer turns number	N_{out}	/	to be determined	calculated	*(3)*
Island half-width	$\mathbf{r_{int}}$	mm	to be determined	variable	
Outer Radius	r_{out}	mm	to be determined	calculated	*(4)*
Straight section length	**L**	mm	to be determined	variable	
Interlayer thickness	$\mathbf{e_{int}}$	mm	to be determined	variable	
Midplane insulation thickness	$\mathbf{e_{mid}}$	mm	to be determined	variable	
2 End Spacers					
Inner spacer axial length	$\mathbf{L_s}$	mm	to be determined	variable	
Outer spacer axial length	$\mathbf{L_{int}}$	mm	to be determined	variable	
Mid-pack turns number	$\mathbf{N_{mid}}$	/	to be determined	variable	

(3) $N_{out} = N_{tot} - N_{int} - N_{mid}$ *(4)* $r_{out} = r_{int} + N_{tot} \times (e_{cbl} + 2.e_{ins})$

***Tab. 2.2.1**: optimization parameters*

It is shown later that the iron parts also play a role in moving the peak field from the heads to the straight. We have soon decided to keep an **amagnetic pole**, so that to keep the flux lines concentrated on the cable itself. Then, **pads and yoke can be at least partly made of iron.** Their 2D shape is kept identical to SD01; the SMC exercise looked at optimising their longitudinal extension along Z axis; this process is described by three additional parameters. The iron B(H) properties are assumed to be the same as "NED iron" [1,i.2].

3D Extension of Iron					
Horizontal pad	$Z_{x\text{-}pad}$	mm	to be determined	variable	
Vertical pad	$Z_{y\text{-}pad}$	mm	to be determined	variable	
Yoke	Z_{yoke}	mm	to be determined	variable	

***Tab. 2.2.2**: 3D optimization parameters*

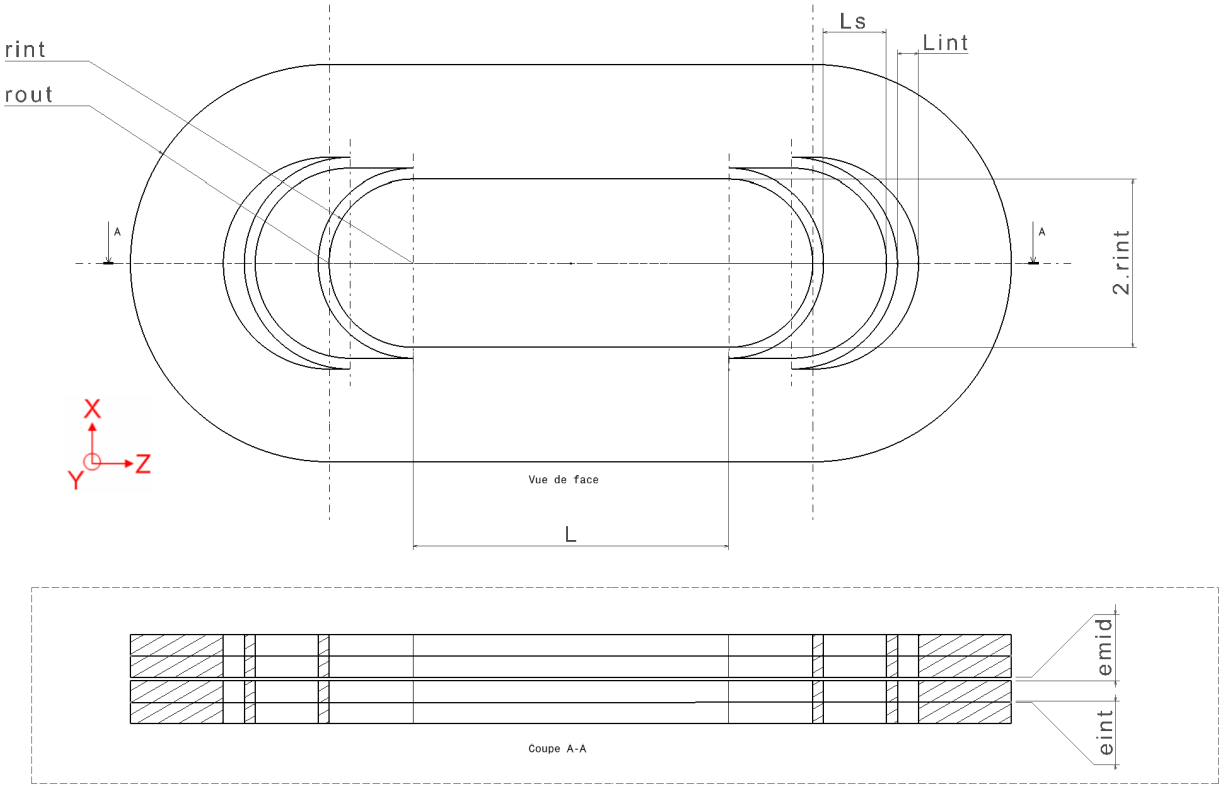

***Fig. 2.2.3**: NED SMC coil pack parameters*

For the coil, initially the general parameters were assumed to be the same as those for the SD01 coils. Later end spacers were introduced with the aim of reducing the magnetic peak in the ends (figure 2.2.3).

2.3- Simulation codes

Three different teams have been working on the magnetic simulations, using their own methods: at CERN, Federico Regis and Paolo Fessia have used **ANSYS® and ROXIE®**; at RAL, James Rochford, Simon Canfer and Elwyn Baynham have worked with **OPERA Vector Fields®**, while Pierre Manil and François Nunio have mainly used **CAST3M** at Saclay. The particularities of every code and the comparison of their results are presented in part 3.

The duplicated calculations served two functions. Primarily they served to validate the computations, and secondly they allowed the different institutions involved to interact and check the validity of their individual modelling processes.

2.4- Magnetic computations steps

The calculations proceeded in a step-by-step manner, repeatedly cross-checking the model results and advancing the design. § 3 is dedicated to those cross-check results and § 4 justifies our final parameters choice for the optimized coils.

First step was to calculate the coil 3D fields without iron and without short sample curve. This preliminary phase was based on comparing the well understood air only calculations and was thus used to confirm each institution was using the chosen parameters in the same manner.

In parallel **2D models with simplified and complete iron assemblies** were implemented in ANSYS. These first models were used to define the overall number of cables to get a peak field B_{max} of about 13 T in the straight section in short sample conditions. The model with complete iron circuit has been used to perform sensitivity study on the assembly materials, on insulation thickness and on air gaps width in order to define the most influent parameters on the peak field. Finally a sensitivity analysis on the yoke width has been carried out once the number of cables has been set, computing the magnetic forces to have a first assessment on the mechanical stresses on the structure. The same model has been used during a second phase to review the overall number of cables, once the pole dimensions have changed for mechanical reasons.

Next improvements have led to **full 3D models with iron**. These final models take into account the short sample limit by scaling linearly the resulting field so that it remains under the superconductor critical curve[4].

The path to final layout was not linear: the first 3D results were iterated back into the calculations, refining the process. This allowed the group to look at the variation of the pole width to avoid cable pop-out on the ends, at a double spacer configuration, at sensitivity studies on iron components' length and at the straight section's extension.

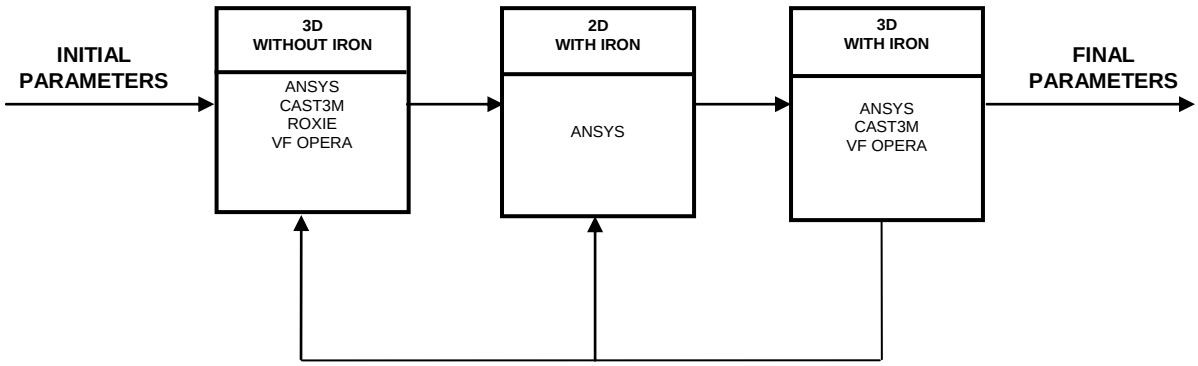

***Fig. 2.4.1**: magnetic computation diagram*

[4] Note that the scaling coefficient and the short sample current are computed from the peak field value. The whole field is then linearly scaled.

3- Cross-check results

3.1- Codes' formulations

a. CAST3M [8]

Field calculations without iron in CAST3M are based on the analytic Biot and Savart formulation. In this context, the source coil is represented as an assembly of block conductors, each of them defined by its geometrical properties. One pancake (1/4 coil) is composed of N+1 packs, where N is the number of spacers in one end. Each pack is divided into two straight parts and two semicircular parts, described by their geometrical properties. The source coil geometry has to be described fully. CAST3M then applies the integrated Biot and Savart formulas on a coil "support mesh" that can be independent from the source coil magnetic definition. This "support mesh" is modelled only in one quadrant (1/8th coil) for symmetry reasons. The resulting "source field" only depends on nodes location, neither on support coil mesh. Surrounding air is not represented in this context. It can be observed that this model is based on a uniform representation of the conductor, showing no difference between cable and insulation. This is coherent with the value of J_{eng} presented in § 2.1. As a consequence, it must be kept in mind that resulting field is only meaningful far from insulation layers.

Iron parts are then added with relevant B(H) curve. Computations now suppose a nonlinear iterative process taking into account iron saturation and surrounding air. Since no infinite boundary condition is available in CAST3M, outer air is represented by a very wide low-meshed box (approximately 2x2 m^2). The assembly is divided into two domains:
- reduced potential area including sources (*i.e.* the coil pack)
- total potential area including iron parts.
The connection surface neither belongs to iron nor to conductor.

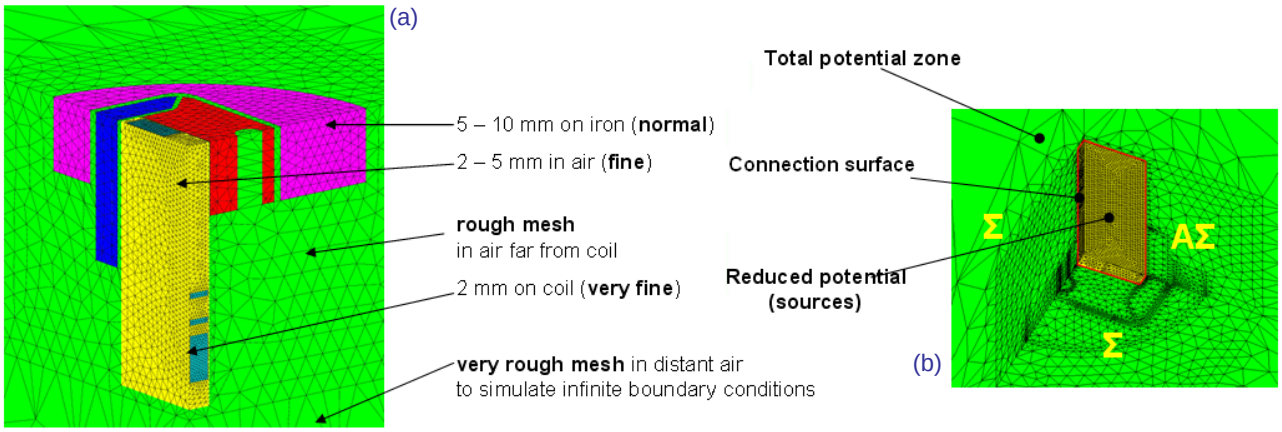

***Fig.3.1.1**: (a) CAST3M model mesh (b) magnetic computation domains (Σ=symmetry ΣA=antisymmetry)*

Those domains need to be homeo-morphed at their interface, *i.e.* to present concordant nodes. In 3D, it is not easy to fulfil such condition with CAST3M since no *free mapping* control of the mesh is available. That's why meshing operation is performed in ANSYS after 'glue' command. Then the mesh description file is converted for CAST3M thanks to a routine created by François NUNIO.

Boundary and interface conditions are set on potential (figure 3.1.1.b). **Calculations are based on magnetic scalar potential approach (MSP)** which corresponds to one degree of freedom A per node. The field source influence is taken into account on the connection surface. CAST3M performs a first linear calculation using the POT_SCAL procedure, providing a starting point. Saturated non-linear iterations are then controlled by the MAG_NLIN procedure using a severe convergence criteria and a high damping ratio[5]. More precisions about MSP theory can be found in references [9,10].

At end, the influence of saturated iron is obtained on each domain in terms of scalar potential. Corresponding field vectors are obtained by applying a gradient function. This solution has to be added to the Biot and Savart "source field" on reduced potential area to get the final solution on the whole assembly.

[5] for CAST3M users, TABB.CRITERE = 1.e-3 ; TABB.OME = .99 ; TABB.ITERMAX = 100 ;

b. ANSYS [11 to 16]

The magnetic vector potential (MVP) formulation and the Magnetic Scalar Potential (MSP) are the two nodal-based methods for 3D static, harmonic, and transient analyses which the ANSYS program supports. Contrary to the MSP, the MVP formulation has three degrees of freedom per node (A_x, A_y, A_z), reducing to one (A_z) if used in 2D static magnetic analyses. ANSYS supports both formulations, but with MVP the current sources can be modelled as an integral part of the finite element model; it is so possible to compute directly the magnetic forces as a combination of the current density J_{eng} and of the flux density B.

The mesh of the coil assembly has to be carefully set up for peak field computations. An element reference size of 2 mm was set, both for 2D and 3D models. These aspects (number of d.o.f. per node and fine mesh) lead to time-demanding simulations for 3D models, both with and without iron assembly. The complexity of the problem is also linked to the constraint equations used to match different mesh zones (*e.g.* coil pack and iron circuit).

Maxwell's equations for magnetostatics and the constitutive equation of magnetic field are solved in terms of vector potential, by employing the Coulomb gauge condition to ensure uniqueness of the vector potential itself. The magnetic flux density, defined as the curl of the magnetic vector potential, is the first derived result, evaluated at the integration points using the element shape functions. The magnetic field intensity *H* is then computed from the flux density *B*, using the *B-H* curve. Nodal values of field intensity and flux density are finally computed from the integration point value.
As a drawback, the vector potential formulation could be incorrect in 3D when the normal component of the vector potential is significant at the interface between elements of different permeabilities. Using a nodal formulation, it is usually assumed that not only the tangential but also the normal component of the vector potential is continuous on any surface, although the latter condition does not follow from any physical consideration. At air/iron interface, the continuous term of the vector potential could be much larger than the discontinuous one and thus the approximation of the discontinuity is numerically difficult.

In order to overcome this problem and at the same time to check the accuracy of the 3D MVP model in terms of peak field and field profile on coil, a 3D MSP model has been realized, based on final configuration parameters. As told before, each node has only one degree of freedom here and current sources are modelled as primitives rather then elements, therefore the current sources do not need to be part of the finite element mesh. Even if only $1/8^{th}$ of the coil is modelled for symmetry reason, the current sources system has to be completely defined like in CAST3M (*cf*. § 3.1.a).

The solver strategy chosen is the Differential Scalar Potential (DSP). The DSP strategy uses a two-step resolution procedure. During first step the magnetic saturation is neglected by imposing a very large value of relative permeability μ in iron regions (set by the solver). The magnetic field intensity H_0 in the iron region is then equal to zero, whereas it is computed in the air and conducting regions after evaluating the source field H_s, produced by the current distribution via integration of Biot and Savart law. Then a scalar potential difference is introduced:

$$\vec{h} = \vec{H} - \vec{H}_0$$

where *H* is the total actual magnetic field. By evaluating the boundary magnetic problem, the difference field is associated to a total scalar potential, defined as continuous in the whole space. Using this potential the magnetic field within the ferromagnetic core can be evaluated without any cancellation error.

The advantage of this formulation is to be much faster than the vector potential one, reducing the simulation time by about 80% with the same element size (2 mm). The only drawback is that no direct computation of magnetic forces can be done without associating each element to a current density value. This problem can be overcome by solving a double step model. The first solves for an electric step, applying a voltage drop on the coil mesh to get the current density distribution; the second one deals with the magnetic solution.

The coil has been realized as a cable stack coil instead of a solid coil as for MVP approach. The bare cable and its insulation have been modelled, associating a different virtual electric resistance proportional to each cable length. At the end of the magnetic step, the Lorentz forces can be obtained at the centroïd of each coil element.

c. ROXIE

The ROXIE[6] program has been developed at CERN for the design and optimization of the LHC superconducting magnets. Within the SMC magnet optimization work, it has been used to study different end spacers' layouts without iron parts. The solver uses Biot and Savart integration of line currents composing each cable, the line currents number being usually equal to the number of strands per cable. Magnetic forces and field profiles on cable have been derived to be compared with the three other programs' results.

d. Vector Fields OPERA

Vector Fields' OPERA program is a general purpose electromagnetic simulation package; within this package the TOSCA algorithm is used to solve magnetostatic and electrostatic problems using a finite element method. It is based on a MSP formulation, using the total magnetic scalar potential in magnetic materials or air regions and the reduced magnetic scalar potential in regions which contain source currents (*cf*. § 3.1.a).

Within reduced potential regions, the field from the source currents are calculated using semi-analytic integration of the Biot and Savart equation. The code represents 'general' conductors as a series of rectangular blocks and/or arcs which have an analytic solution and more general conductor shapes using 8 or 20-node isoperimetric finite elements to represent the conductor. The accuracy of the field computation within the coil elements can be specified, the code uses an adaptive integration procedure to achieve the desired accuracy. The field from any coil can be generated by superposition of these sub-elements fields.

Total scalar potential should be used in regions containing permeable materials; the field contribution from non-linear iron is then calculated iteratively using the iron properties and the calculated source fields. The non-linear material characteristics – B(H) data – are entered as a table of point values or as an algebraic function.

On the interface between the total and reduced potential spaces, the two potentials are linked together by applying the conditions of normal *B* and tangential *H* continuity. This involves the evaluation of the normal and tangential field produced by the conductors on the surface; a scalar potential is then used to represent the tangential field on the interface surface.

Both regions are meshed, however the conductor entities do not form part of the mesh, the effects of their fields are mapped to the interface surface between the total and the reduced potentials that contain them, as described above. The contribution from the coil fields and the iron regions are added together in the post processing module to generate the final field distribution. The iron fields can be calculated directly from the finite element potential solution (nodally averaged) or by integration from the material magnetisation (calculated from the finite element solution).

Reflections and rotations can be used to exploit any natural electromagnetic symmetry, this reduces the problem size. Boundary conditions must be imposed on all free surfaces of the finite element mesh and far field boundaries where the mesh is truncated can be represented by a Kelvin transformation.

It's interesting to highlight how similar this computation sequence is to CAST3M's one.

[6] Routine for the Optimization of magnet X-sections, Inverse field computation and coil End design

3.2- Solutions comparison

a. First checks

To assure reliable and coherent comparisons, it was necessary to cross-check the four initial models.

Precise coil parameters for these models are not given here: the results are presented to show to what extent the models agreed. Magnetic field has been computed for an intensity of 17180 A corresponding to I_c=2500 A.mm^{-2}, without taking into account here the short sample critical current curve[7]. That's why such high values (around 17 T) are observed.

The first check was to make sure that the conductor volumes and the current densities were the same in every model. Following this the fields predicted by the models were compared.

The accompanying table 3.2.1 compares those values. The cross-check was very encouraging at this step. It can be seen that the results are quasi identical on conductor between CAST3M, ROXIE and Vector Fields. A slight difference is observed with ANSYS (lower than 2%) and this was identified as a peak effect, linked to the mesh, which is not observed in regions away from maxima.

Code	B_0	B_{ss}	B_{head} (inner pack)	B_{head} (outer pack)	ΔB_{ss}
CAST3M	(13.43)[8]	15.16	16.34	16.90	1.74
VF OPERA	12.94	15.16	16.52	16.88	1.72
ROXIE	12.95	15.22	16.22	16.64	1.42
ANSYS MVP	12.92	14.87	16.25	16.42	1.55
ANSYS MSP	13.01	15.23	16.57	16.92	1.69

***Tab.3.2.1**: comparison between peak field values in the 'no iron' case at 17 kA (all values in T)*

b. Full model comparison

These are the results of the first full model checks: **note this model is not optimised and does not allow for the critical curve.** It serves as a check on the similarities of the code computations[9].

The models are crosschecked in the {Z=0} and {X=0} planes by plotting and comparing the resulting fields. Figure 3.2.2 illustrates the locus of the plots, while the comparisons themselves are shown in figure 3.2.3.

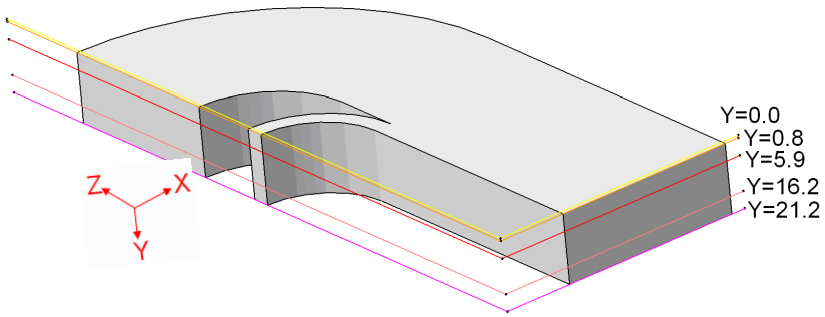

***Fig.3.2.2**: cross-check test-lines*

[7] thus, the results have no physical signification, they are just a base for comparisons.
[8] B_0 value is not significant in the CAST3M model. The reason of this discrepancy is explained in § 3.3.
[9] for instance, cross-check configuration only presents one end spacer whereas final configuration will be based on two spacers.

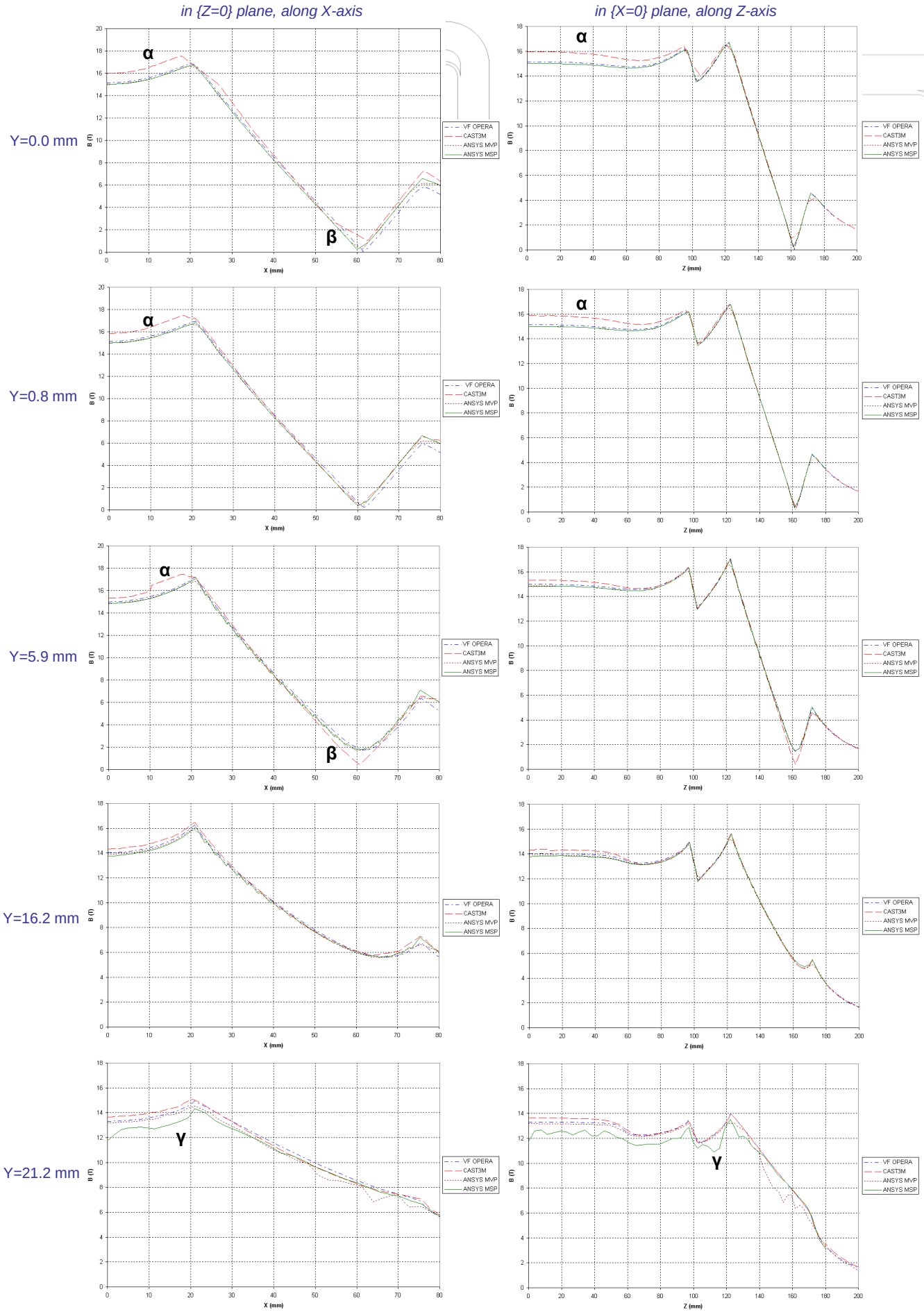

***Fig.3.2.3**: cross-check results between 4 formulations on ten test-lines (non-linear case with iron) at 17 kA*

3.3- Comparison analysis

A first glance shows all of the curves are comparable, which reveals a good agreement between the models. A more careful inspection shows that this agreement is remarkably good on the coil. In particular, the peak field values in {X=0} plane are identical for all the models, with less than 2% difference (apart for Y=21.2 mm). This result is very positive, giving confidence in the resulting peak values, which are critical to the magnetic specification.

Nevertheless, there are discrepancies, mainly in air, that need to be explained.

A visual analysis of previous plots leads to the definition of three types of discrepancies:
- **Type α** corresponds to an important overestimation of the field in air with CAST3M, close from symmetry planes (up to +0.5 T). This effect vanishes when Y increases, and does not affect the field values on coil. A discontinuous singularity is observed for Y=5.9 mm.
- **Type β** corresponds to an occasional field underestimation around its minimum.
- **Type γ** corresponds to variations of the field evolution with ANSYS (MSP and MVP) observed only for Y=21.2 mm.

β discrepancies can be simply explained by a mesh effect: values on the test-line are obtained by an arithmetic projection of the surrounding node's values (*PROI* command in CAST3M). The resulting value depends on the mesh size, and of the test-line position inside the element. That's why β discrepancies are only observed sometimes, depending on the relative position of the test-line and the crossed elements.

γ discrepancies are proper to the ANSYS model, for both formulations. The erratic modulations of the field appear at the boundary between the coil and the outer air (Y=21.2 mm), where two different mesh patterns are matching through constraint equations which relate master to slave nodes. The outer mesh has 4 mm brick element size, whereas the conductor size is about 2 mm. Nevertheless this element size has been set as the best compromise between peak field precision and time-saving simulations. The resulting field pattern at the boundary between coil and air can so be considered as a localized imprecision.

α overestimations are confined to the CAST3M model. Observing the Y=5.9 mm plot shows part of the explanation. The discontinuity corresponds to a situation where the test-line crosses air elements which have at least one node located on the symmetry plane (marked with green arrows). Those elements are called "erratic" and represented in yellow in figure 3.3.1:

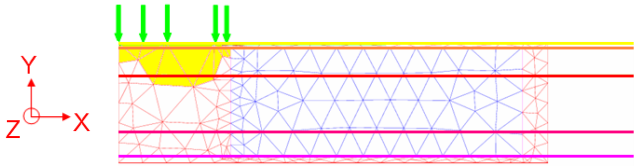

Fig.3.3.1*: cut of {Z=0} plane showing test-lines and erratic elements in CAST3M*

In the same way, the overestimation for Y=0 and 0.8 mm corresponds to a cross of erratic elements. This error is linked to the symmetry plane. After nonlinear computation, the solution is obtained in terms of potential. To get the magnetic field, a gradient must be applied. In CAST3M, the *GRAD* procedure realizes an estimation of the gradient on one node by using the numeric differences with the surrounding nodes. On the symmetry plane, the number of surrounding nodes is reduced (symmetric nodes are not represented), so the weighted mean realized by *GRAD* exaggerates the influence of the gradient in the plane direction. This fictively increases the tangential gradient in the solution, which leads to a systematic overestimation of the field inside the erratic elements. Fortunately in our case, the coil mesh (in blue) is not linked to erratic nodes, so the error is localized on air.

3.4- Cross-check conclusions

The cross-check has proved to be successful and shows that the four models agree very well. There are discrepancies between the codes, however within the context of this evaluation these are trivial and do not affect the peak field values on the coil which are central to defining the short prototype coils. Furthermore the differences observed have been fully understood.

This comparative study showed the optimisation of the SMC short prototype coils could proceed with confidence.

4- Magnetic optimized results

4.1- Parameters influence

a. First simulations

Optimization target is to minimize (B_{max}-B_{ss}) under constraint of 0.5T, aiming to get B_{max}>13 T. A series of optimizations without iron were performed, to isolate the influence of each parameter (following plots are shown for illustration; note not all the parameters' values for each model are shown). Following this study the following conclusions were drawn:

- **The use of spacers is mandatory**

- **N_{int}=2 is optimal** to lower ΔB_{ss}

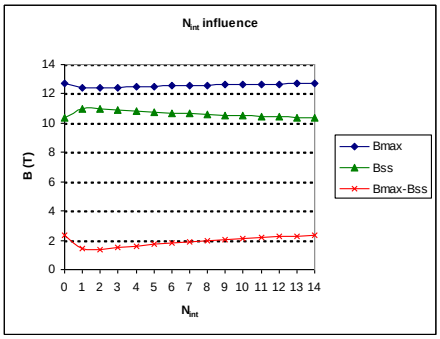

(a)

- **Insulation thicknesses (e_{mid} and e_{int}) were seen to play a negligible role on resulting field**: a maximum of 0.4% difference is observed on peak field if the midplane insulation is 1.6 mm-thick instead of SD01's 2.7 mm (e_{mid}). A 0.2 mm-thick insulation sheet will be inserted in between the two coil layers, according to LBNL experience (e_{int}).

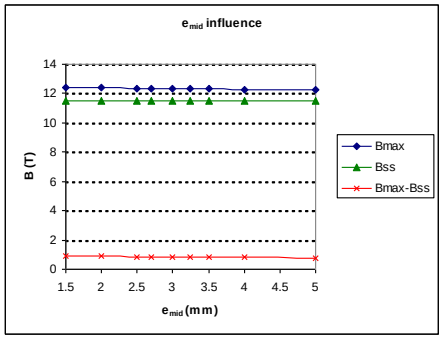

(b)

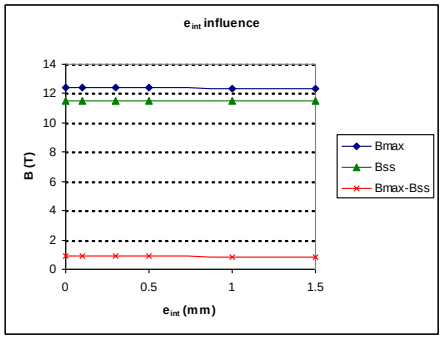

(c)

Fig. 4.1.1: *CAST3M 3D simulations without iron (a) inner turns number influence (b) midplane insulation thickness influence (c) interlayer insulation thickness influence*

- **N_{tot}≥20 to get B_{max}>13 T**. The short sample condition was computed by linear interpolation next to the load line and then numerically checked. Analyses on the component materials reveal that to get the target field, both the pads have to be made from iron. The final value of 21 cables was set to give a margin of 2% on peak field, this allowed for numerical uncertainties in the calculation.

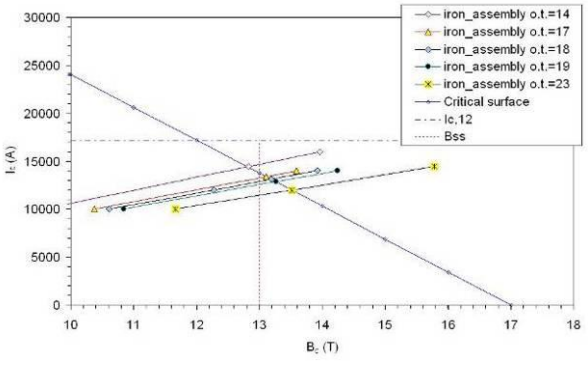

(a)

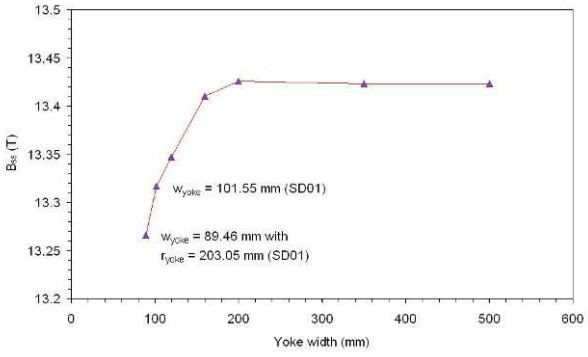

(b)

Fig. 4.1.2: *ANSYS 2D simulations (a) total turns number influence (b) yoke width influence*

- increasing L reduces the ends effect on straight section and improves the field uniformity. On the other hand, L and L_s must remain short enough to make sure that the coil pack fits to the furnace available.

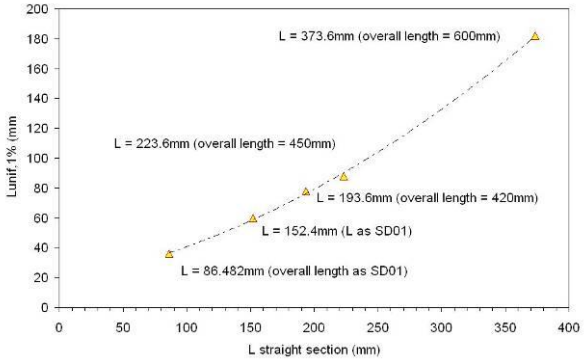

Fig. 4.1.3: *ANSYS 3D: straight section length influence on field uniformity*

- In order to decrease the peak field on the coil ends and to keep the maximum field on the inner pack, **the spacer length L_s should be larger than 20 mm**. In this case the maximum field loss is about 3% compared to a simple racetrack coil and the peak field moves to the outer pack. Longer spacers do not improve this situation.

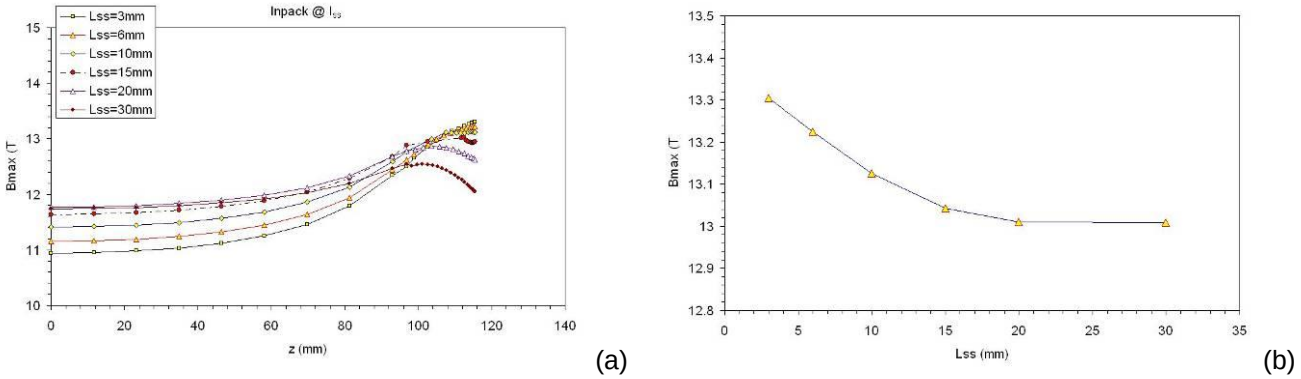

(a) (b)

Fig. 4.1.4: *ANSYS 3D simulations (a) peak field on inner pack as a function of spacer length at short sample (b) peak field on coil as a function of L_s*

- r_{int} should be as small as possible in terms of magnetic efficiency. Nevertheless, **it needs to be large enough to avoid bending issues, such as cable pop-outs**. SD01 coil presented an insulated cable thickness of 1.475 mm and an internal radius of 18.6 mm. From this experience, we consider that 32.8 mm (scaled value of the radius) is the minimal value. Later it was decided to allow a margin by setting r_{int} to 40 mm. This conservative stance was adopted because the SMC had not carried out any bending trials. The increase of pole width leads to a decrease of the axial magnetic resultant F_x with benefit in term of axial stress σ_x on cable, whereas F_y increases.

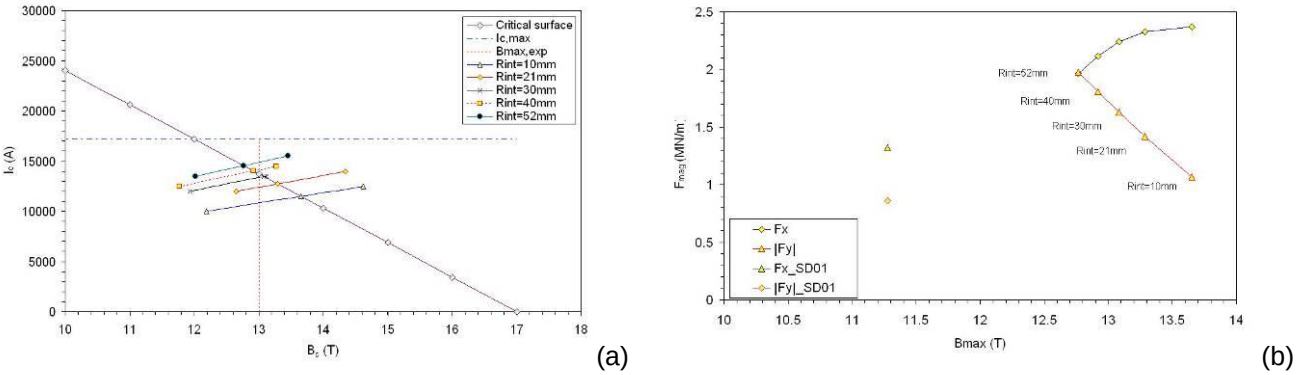

(a) (b)

Fig. 4.1.5: *(a) total number of cables has been plotted as a function of the central pole width (w_{yoke} = 90 mm as for SD01) (b) magnetic forces as a function of the pole width: F_x increases of 60% and F_y of 110% with respect to SD01 (r_{int} = 40 mm)*

After the preliminary calculations, the peak field still remained located on ends. This is mainly due to the initial constraint on L_{tot}<420 mm. The goal following thus was to move this to the straight of the coil.

b. Iron parts influence

The first iron calculations show that an amagnetic island was essential (*i.e.* z_{pole}=0), contrary to SD01 case. Indeed, an iron pole concentrates the magnetic flux inside the coil and reduces the effect of external iron parts. In SD01, the X-pad length covers the whole coil length, whereas Y-pad and iron yoke length is shorter than coil straight section length (*cf*. figure 4.1.6). In this way the peak field is moved to straight section with a difference ΔB equal to 0.2 T.

The use of longer lateral pads over the coil axial length has proven its efficiency in terms on SMC: **peak can be moved in straight part**, but a longer straight section is mandatory (as computation in air showed before). A different vacuum furnace is chosen (at Culham), wide enough to free the SMC initial dimensional constraints, both in terms of coil length and pole width. The best configuration with single spacer leads to a ΔB of 0.3 T at short sample, with {L=300 mm, L_s=15 mm}, still below our target of 0.5 T.

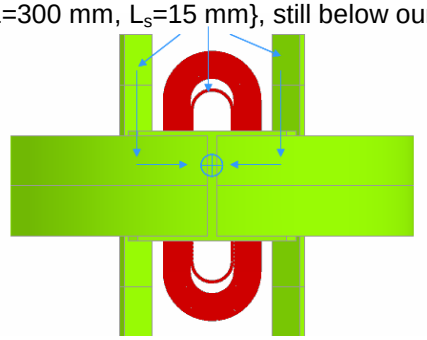

Fig. 4.1.6*: extended X-pad influence on magnetic flux circulation (Vector Fields OPERA)*

c. Two-spacer configuration

To increase the ΔB between the end field and the straight, a double spacer configuration was explored. Different spacers' lengths for lower and upper layers, keeping either the same coil outer dimensions or the same straight section length were examined. The first of these leads to a complication in pole design since it causes the design to have the layer jump on straight section thus affecting the cable mechanical homogeneity where the peak field occurs. This is not desirable. On the other hand, the second choice leads to a more complicated design of the coil containing structure. **The final configuration will adopt identical end spacers for both layers.** The layout proposed is: 2 turns for the inner pack, 2 for the mid- and 17 for the outer one.

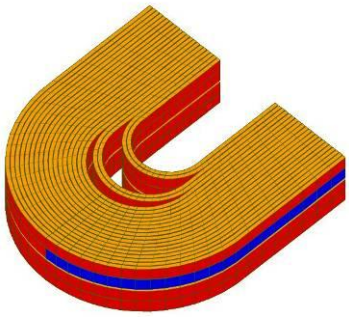

(a)

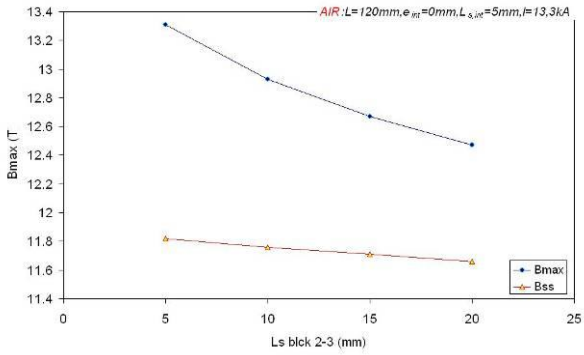

(b)

Fig. 4.1.7*: (a) double spacer configuration (ROXIE) (b) B_{max} and B_{ss} trend as functions of the spacer between block 2 and 3. The first spacer length has been set to 5 mm and the straight section length to 120 mm*

This configuration was included with the iron circuit configuration described above, and then validated by checking it with a length **L_s of 30 mm for the inner spacer and L_{int}=10 mm for the outer one**. That latter value is the minimal size to ensure mechanical feasibility. **L was fixed at 150 mm, based on our earlier studies**. The peak field difference on the inner pack increases using this layout while bringing the mid- and outer packs head peak at straight's connexion.

To get a confirmation of the second spacer's influence, a comparison has been made between one and two-spacers cases, for {L_s=30 mm; L_{int}=10 mm} and {L_s=40 mm; L_{int}=0} values. It is confirmed that field properties are similar in straight section (same peak value for *Z=0*). Second spacer plays a determining influence on field repartition on mid-pack (turns 3 and 4): it moves the head peak field from centre of the end to the straight connexion. Meanwhile, head peak is reduced from 12.773 to 12.220 T with the second spacer at short sample. This brings ΔB_{ss} from 0.148 to 0.702 T. This shows the use of a second spacer is necessary to reach the 0.5 T field difference desired.

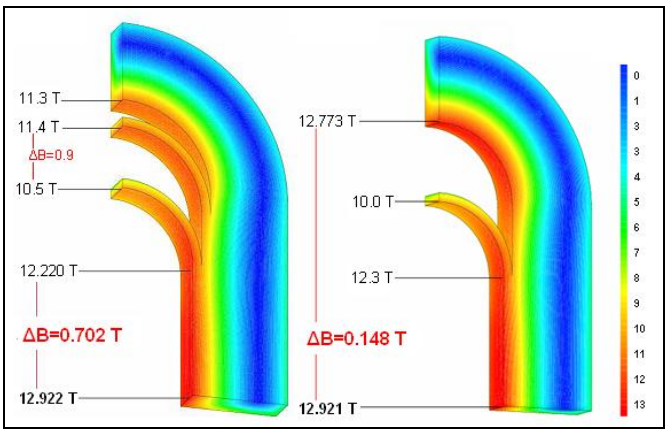

***Fig. 4.1.8**: resulting field comparison between 1- and 2-spacer cases (at short sample: 14 kA, CAST3M)*

4.2- Final choice

The final coil pack parameters can now be defined and are presented in table 4.2.1:

Parameter	Name	Unit	Value	d.o.f.	Notes
Coil Pack – Double Pancake Configuration					
Turns number	$\mathbf{N_{tot}}$	/	21	fixed	
Inner turns number	$\mathbf{N_{int}}$	/	2	fixed	
Mid-pack turns number	$\mathbf{N_{mid}}$	/	2	fixed	
Outer turns number	N_{out}	/	17	calculated	
Island half-width	$\mathbf{r_{int}}$	mm	40	fixed	
Outer Radius	r_{out}	mm	94.6	calculated	
Straight section length	**L**	mm	150	fixed	
Interlayer thickness	$\mathbf{e_{int}}$	mm	0.2	fixed	
Midplane insulation thickness	$\mathbf{e_{mid}}$	mm	1.6	fixed	
2 End Spacers					
Inner spacer axial length	$\mathbf{L_s}$	mm	30	fixed	
Outer spacer axial length	$\mathbf{L_{int}}$	mm	10	fixed	
Coil Dimensions					
Overall length	L_{tot}	mm	419.2	calculated	*(5)*
Overall width	w_{tot}	mm	189.2	calculated	*(6)*
Overall thickness	e_{tot}	mm	42.4	calculated	*(7)*

(5) $L_{tot} = L + 2.r_{int} + 2.N_{tot} \times (e_{cbl} + 2.e_{ins}) + 2.L_s + 2.L_{int}$ *(6)* $w_{tot} = 2.r_{out}$ *(7)* $e_{tot} = 4.(w_{cbl} + 2.e_{ins}) + e_{mid} + 2.e_{int}$

***Tab. 4.2.1**: final coil pack properties*

Iron parts longitudinal extensions are set as follow:

3D Extension of Iron					
Horizontal pad	$z_{x\text{-}pad}$	mm	210	fixed	=140% L
Vertical pad	$z_{y\text{-}pad}$	mm	105	fixed	=70% L
Yoke	z_{yoke}	mm	105	fixed	=70% L

Note: some minor changes may happen on those theoretical values during the mechanical optimization

***Tab. 4.2.2**: final iron parts extensions*

4.3- CAST3M predicted field values - MSP

Using the CAST3M MSP formulation, the SMC model gives a peak field B_{max} of 12.92 T at inner pack straight section, 0.702 T higher than in the inner pack ends, where the maximum field reaches 12.22 T at end/straight section connection.

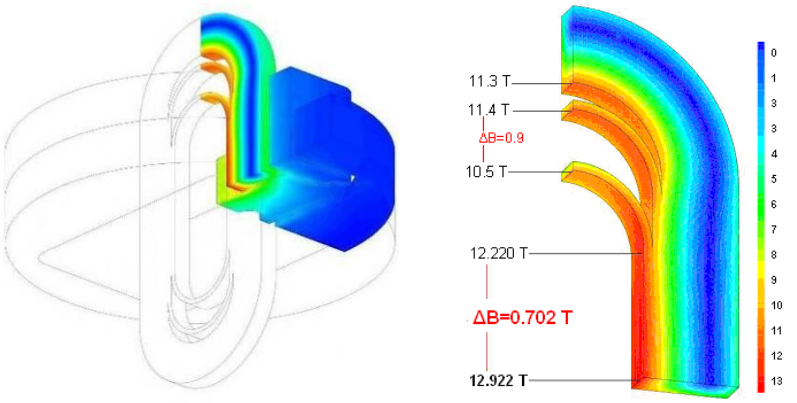

***Fig. 4.3.1**: magnetic flux density on coil pack at short sample (I_{ss} = 14.01 kA)*

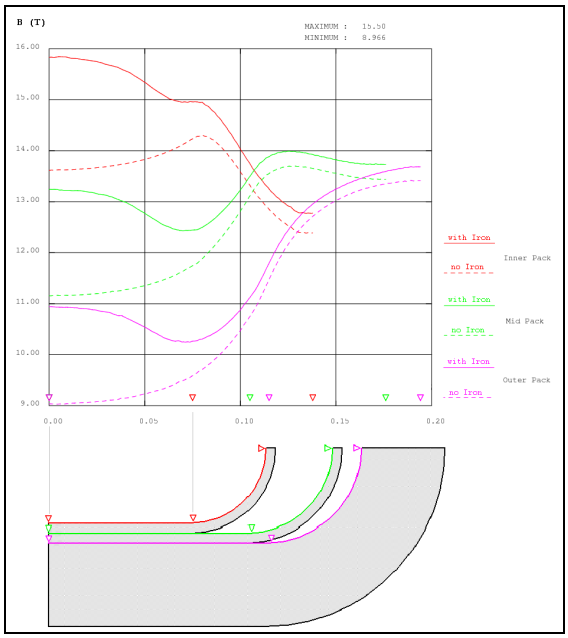

***Fig. 4.3.2**: field evolution along 3 packs' inner turn at 17 kA with and without iron*

This figure shows the peak field location at 17 kA, the field uniformity and of the difference observed with ends. It is also interesting to see the influence of the iron parts that manage to increase significantly the field in central plane to reach our specifications.

Lorentz forces - Energy			
X-Force on 1/8th coil	F_x	kN	328
Y-Force on 1/8th coil	F_y	kN	-393
Z-Force on 1/8th coil	F_z	kN	131
X-Force on straight section	F_x^{2D}	MN.m^{-1}	1.9
Y-Force on straight section	F_y^{2D}	MN.m^{-1}	-1.8
Total stored magnetic energy	E_{mag}	kJ	211[10]
Magnet inductance	$\mathscr{L}$	mH	2.1

***Tab. 4.3.3**: magnetic forces and energy at short sample (I_{ss} = 14.01 kA)*

[10] Stored energy is calculated by hand in CAST3M using the permittivity values after last iteration (accessible with *tabb.TABNUSEC.obfer1.klast*), before integrating $\mu.H^2/2$ on the whole domain ; L is such that $2.E_{mag}=L.I_{ss}^2$.

4.4- ANSYS predicted field values - MVP

Using the MVP formulation, the SMC model gives a peak field B_{max} of 12.85 T at inner pack straight section, 0.706 T higher than in the inner pack ends, where the maximum field reaches 12.2 T at end/straight section connection.

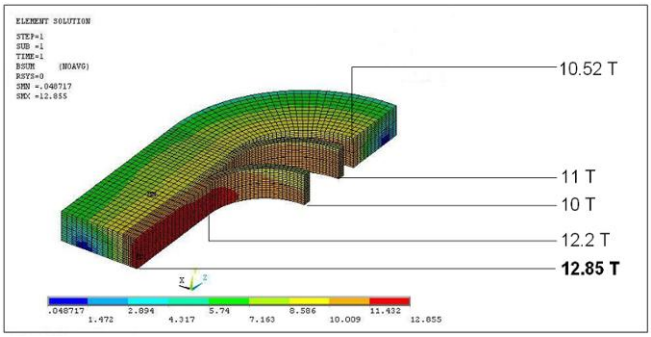

***Fig. 4.4.1**: magnetic flux density on coil pack at short sample (I_{ss} = 14.25 kA)*

Lorentz forces - Energy			
X-Force on 1/8th coil	F_x	kN	338
Y-Force on 1/8th coil	F_y	kN	-406
Z-Force on 1/8th coil	F_z	kN	136
X-Force on straight section	F_x^{2D}	MN.m^{-1}	2.06
Y-Force on straight section	F_y^{2D}	MN.m^{-1}	-1.95
Total stored magnetic energy	E_{mag}	kJ	198
Magnet inductance	$\mathscr{L}$	mH	2.0

***Tab. 4.4.2**: magnetic forces and energy at short sample (I_{ss} = 14.25 kA)*

4.5- ANSYS predicted field values - MSP

Using the MSP formulation, the SMC model gives a peak field B_{max} of 12.94 T at inner pack straight section, 0.714 T higher than in the inner pack ends, where the maximum field reaches 12.22 T at end/straight section connection.

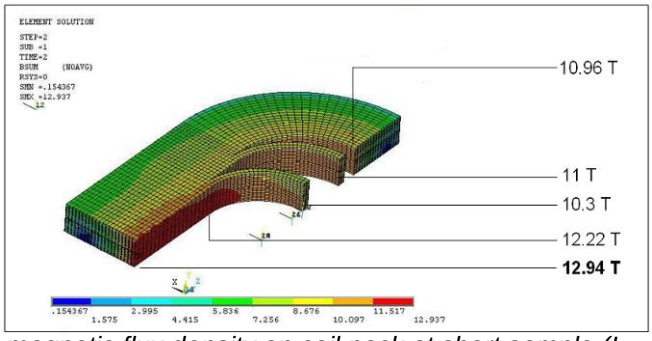

***Fig. 4.5.1**: magnetic flux density on coil pack at short sample (I_{ss} = 13.96 kA)*

Lorentz forces - Energy			
X-Force on 1/8th coil	F_x	kN	326
Y-Force on 1/8th coil	F_y	kN	-388
Z-Force on 1/8th coil	F_z	kN	131
X-Force on straight section	F_x^{2D}	MN.m^{-1}	1.98
Y-Force on straight section	F_y^{2D}	MN.m^{-1}	-1.86
Total stored magnetic energy	E_{mag}	kJ	190
Magnet inductance	$\mathscr{L}$	mH	1.9

***Tab. 4.5.2**: magnetic forces and energy at short sample (I_{ss} = 13.96 kA)*

4.6- Vector Field OPERA predicted field values - MSP

Using Vector Fields package, the SMC model gives a peak field B_{max} of 12.96 T at inner pack straight section, 0.73 T higher than in the inner pack ends, where the maximum field reaches 12.23 T at end/straight section connection.

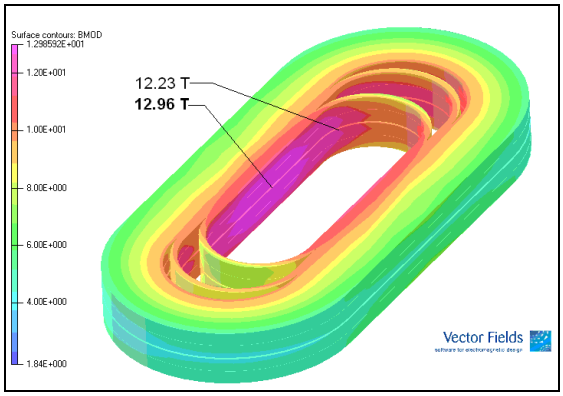

***Fig. 4.6.1**: magnetic flux density on coil pack at short sample (I_{ss} = 14.00 kA)*

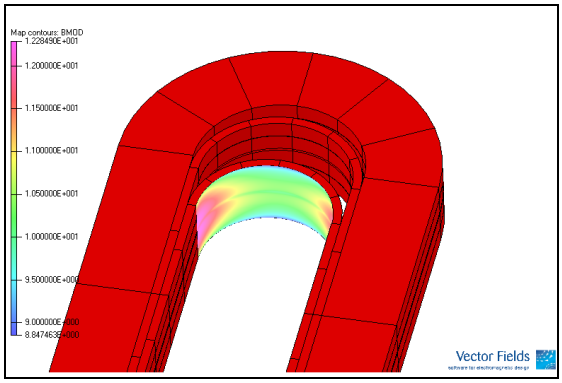

***Fig. 4.6.2**: how the field varies on the inside surface of the inner pack end*

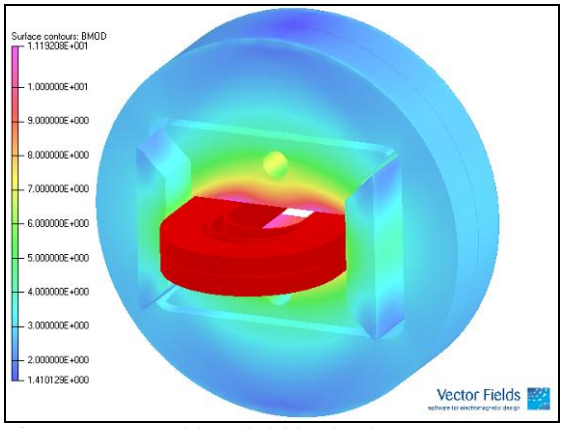

***Fig. 4.6.3**: resulting field in the iron components*

Lorentz forces - Energy			
X-Force on 1/8th coil	F_x	kN	333
Y-Force on 1/8th coil	F_y	kN	-396
Z-Force on 1/8th coil	F_z	kN	132
X-Force on straight section	F_x^{2D}	MN.m^{-1}	2.0
Y-Force on straight section	F_y^{2D}	MN.m^{-1}	-1.9
Total stored magnetic energy	E_{mag}	kJ	209
Magnet inductance	$\mathscr{L}$	mH	2.1

***Tab. 4.6.4**: magnetic forces and energy at short sample (I_{ss} = 14.00 kA)*

5- Conclusions and next steps

First step of NED SMC project has led to an efficient coil pack configuration presenting a high magnetic field with its maximum located on the straight section, this with a significant margin compared to ends field as summed up in the table 5.1. This enables the quenches in ends to be limited and as a consequence it should now be possible to reach higher currents in the coil during our training studies.

Parameter	Name	Unit	Specif	values at short sample				Valid	Notes
				CAST3M MSP	ANSYS MVP	ANSYS MSP	OPERA MSP		
Magnetic Field Key Values									
Peak field	B_{max}	T	≥13	**12.92**	**12.85**	**12.94**	**12.96**	OK	*1% tolerance*
				in straight section					
End peak field	B_{end}	T	none	12.22	12.20	12.22	12.23	free	
Uniform field zone length	$L_u^{1\%}$	mm	~60	~70	~55	~55	~60	OK	*at 1% in z*
B_{ss} - B_{end}	ΔB_{ss}	T	≥0.50	0.70	0.71	0.71	0.73	OK	
$B_{end}^{(inner\ pack)}$ - $B_{end}^{(outer\ pack)}$	ΔB_{end}	T	≥0.5	0.9	1.0	1.3	0.9	OK	
Central field	B_0	T	none	9.93	9.85	9.65	NC	free	
Facilities									
Short sample current	I_{ss}	kA	≤20	14.01	14.25	13.96	14.00	OK	
Overall length	L_{tot}	mm	**419.2**					OK	*without tooling*
Overall width	w_{tot}	mm	**189.2**					OK	*without tooling*
Overall thickness	e_{tot}	mm	**42.4**					OK	*without tooling*
Overall cable length	L_{cbl}	m	**73**					OK	*per assembly*

***Tab. 5.1**: final magnetic field properties at short sample: comparison between 3 formulations*

Using SD01 as a starting point, SMC study has shown:
- increasing the coil general dimensions (thanks to larger furnace capacity)
- using an amagnetic island
- reshaping the iron parts
- using four appropriate end spacers

The magnetic field computations have been rigorously validated: it's now possible to calculate the 3D Lorentz forces field and to start mechanical computations, aiming at sustaining the internal coil forces and at getting the pre-stress range desired. A final iteration will be needed once the real strand current density limit is known. This parametric model will obviously be available to evaluate the resulting field if some coil parameters happen to change. It will be useful if some dipoles are wound with a different cable in the future.

On a technical level, our cross-checks have validated that the use of ANSYS, CAST3M and OPERA for magnet design leads to common conclusions.

Acknowledgements

The SMC working group would like to thank everyone involved in the magnetic optimization described in this paper, especially Ray HAFALIA at Berkeley for his advice on the coil and support design and Chhon PES at Saclay for its support with the magnetic modelling.

Tables and figures

Acronyms and symbols

Symbol	Meaning
AT	Accelerator Technologies
B&S	Biot and Savart
CARE	Coordinated Accelerator Research in Europe
CEA	Commissariat à l'Énergie Atomique
CERN	European Organization for Nuclear Research
DSP	Differential Scalar Potential
IRFU	Institut de Recherche sur les lois Fondamentales de l'Univers
JRA	Joint Research Activity
LARP	LHC Accelerator Research Program
LBNL	Lawrence Berkeley National Laboratory
LHC	Large Hadron Collider
MSP	Magnetic Scalar Potential
MVP	Magnetic Vector Potential
NED	Next European Dipole
RAL	Rutherford Appleton Laboratory
ROXIE	Routine for the Optimization of magnet X-sections, Inverse field computation and coil End design
SACM	Service des Accélérateurs et du Cryo-Magnétisme
SD01	Subscale Dipole #1
SIS	Service d'Ingénierie des Systèmes
SMC	Short Model Coils
α_c	Critical current slope at 12 T
A, A_x, A_y, A_z	Magnetic potential degrees of freedom
ΔB_{ss}	Difference between straight section and end peak fields
ΔB_{end}	Difference between end packs peak fields
$Ø_{str}$	Strand diameter in cable
B_0	Central magnetic field
B_{max}	Peak magnetic field
B_{end}	End peak magnetic field
e_{cbl}	Cable thickness at 20 MPa
e_{ins}	Cable insulation thickness per face
e_{int}	Interlayer insulation thickness
E_{mag}	Total stored magnetic energy (on full magnet)
e_{mid}	Midplane insulation thickness
e_{tot}	Overall thickness
F_x, F_y, F_z	Force component on 1/8th coil
F_x^{2D}, F_y^{2D}	Force component on straight section
fil_{-X}	Gap between pads
fil_{-Y}	Insulation thickness between Y-pad and coil
gap_{-X}	X-pad / Yoke air gap thickness
gap_{-Y}	Y-pad / Yoke air gap thickness
I_c^{12}	Practical current (at 2500 A.mm^{-1})
I_c^{trg}	Target current (at 3000 A.mm^{-1})
I_{ss}	Working current
J_{eng}	Insulated cable practical current density at 17 180 A
L	Straight section length (on inner pack)
$\mathscr{L}$	Magnet inductance
L_{cbl}	Overall cable length
L_{int}	Outer spacer axial length
L_s	Inner spacer axial length
L_{tot}	Overall length
$L_u^{1\%}$	Uniform magnetic field zone length
N_{int}	Inner turns number
N_{mid}	Mid-pack turns number
N_{out}	Outer turns number
N_{str}	Number of strands in cable
N_{tot}	Overall turns number
p	Twist pitch
$r_{Cu/nCu}$	Copper / non-copper rate in cable
r_{int}	Island half-width
r_{out}	Outer radius
r_{yoke}	Yoke radius
w_{cbl}	Cable width
w_{hs}	Horseshoe lateral width
w_{tot}	Overall width
$Z_{x\text{-}pad}$	X-pad iron longitudinal extension
$Z_{y\text{-}pad}$	Y-pad iron longitudinal extension
Z_{yoke}	Yoke iron longitudinal extension
Z_{pole}	Pole iron longitudinal extension

References

[1] **A. DEVRED *et al.***
Overview and status of the Next European Dipole Joint Research Activity
Supercondu. Sci. Technol. 19 (2006) S67-S83

[2] **S. CASPI, S. GOURLAY, R. HAFALIA, A. LIETZKE, J. ONEILL, C. TAYLOR, A. JACKSON**
The use of pressurized bladders for stress control of superconducting magnets
IEEE Transactions on Applied Superconductivity, Vol. 11, No. 1, March 2001

[3] **R.R. HAFALIA, S. CASPI, L. CHIESA, M. COCCOLI, D.R. DIETDERICH, S. A. GOURLAY, A.F. LIETZKE, J.W. O'NEILL, G. SABBI, AND R.M. SCANLAN**
A new support structure for high field magnet
IEEE Transactions on Applied Superconductivity, Vol. 12, No. 1, March 2002, pp. 47-50

[4] **R.R. HAFALIA, P.A. BISH, S. CASPI, D.R. DIETDERICH, S.A. GOURLAY, R. HANNAFORD, A.F. LIETZKE, N. LIGGINS, A.D. MCINTURFF, G.L. SABBI, R.M. SCANLAN, J.W. O'NEILL, J.H. SWANSON**
An Approach for Faster High Field Magnet Technology Development
IEEE Transactions on Applied Superconductivity, Vol. 13, No. 2, June 2003, pp. 1258-1261.

[5] **F. RONDEAUX**
Insulation development: final report on innovative insulation
CARE-Report-2007-037-NED, Dec. 2007, CEA Saclay, France

[6] **H. FÉLICE**
Contribution à la conception des bobinages supraconducteurs de type dipolaire en Nb_3Sn pour les accélérateurs de particules
Rapport de thèse CEA DAPNIA-06-09-T; thèse soutenue le 12/10/2006

[7] **G. AMBROSIO *et al.***
Design of the first LARP long racetrack magnet (LRS01)
LARP_SRDnote_02; Nov. 2006; edited at Fermi National Accelerator Laboratory, Technical Division, Magnet System Dpt

[8] **P. VERPEAUX, T. CHARRAS, A. MILLARD**
Castem2000: une approche moderne du calcul des structures
in Calcul des Structures et Intelligence Artificielle, P. 261. Pluralis, 1988

[9] **C. W. TROWBRIDGE**
An Introduction to Computer Aided Electromagnetic Analysis
Vector Fields Limited, Oxford, England, 1990

[10] **P. MANIL**
CAST3M : Application à l'optimisation de bobines dipolaires Nb_3Sn modèle réduit
talk Club CAST3M 2008, Nov. 2007, Paris

[11] **ANSYS USER GUIDE**

[12] **M. GYIMESI, D. OSTERGAARD**
Non-conforming hexahedral edge elements for magnetic analysis
IEEE Transactions on Magnetics, Vol. 34, No. 5, September 1998, pp. 2481-2484.

[13] **K. PREIS, I. BARDI, O. BIRO, C. MAGELE, G. VRISK, K.R. RICHTER**
Different finite element formulations of 3D magnetostatic fields
IEEE Transactions on Magnetics, Vol. 28, No. 2, March 1992, pp. 1056-1059.

[14] **I.D. MAYERGOYZ**
A new scalar potential formulation for three dimensional magnetostatic problems
IEEE Transactions on Magnetics, Vol. MAG-23, No. 6, November 1987, pp. 3889-3894.

[15] **M.G. GYIMESI, D. LAVERS, T. PAWLAK, D. OSTERGAARD**
Application of the general potential formulation
IEEE Transactions on Magnetics, Vol. 29, No. 2, March 1993, pp. 1345-1347.

[16] **K. PREIS, I. BARDI, O. BIRO, C. MAGELE, W. RENHART, K.R. RICHTER, G. VRISK**
Numerical analysis of 3D magnetostatic fields
IEEE Transactions on Magnetics, Vol. 27, No. 5, September 1991, pp. 3798-3803.

Internet references:

[i.1] http://lt.tnw.utwente.nl/research/HCS/Projects/CARE-NED/
Official CARE-NED project homepage

[i.2] https://edms.cern.ch/
NED SMC Project database; note, presentations and Minutes available *[restricted access]*